LIGHT DIFFRACTION STUDIES OF SINGLE MUSCLE FIBERS AS A FUNCTION OF FIBER ROTATION

WOLFGANG G. GILLIAR, WILLIAM S. BICKEL, AND WILBUR F. BAILEY
Physics Department, University of Arizona, Tucson, Arizona 85721

ABSTRACT Light diffraction patterns from single glycerinated frog semitendinosus muscle fibers were examined photographically and photoelectrically as a function of diffraction angle and fiber rotation. The total intensity diffraction pattern indicates that the order maxima change both position and intensity periodically as a function of rotation angle. The total diffracted light, light diffracted above and below the zero-order plane, and light diffracted into individual orders gives information about the fiber's longitudinal and rotational structure and its noncylindrical symmetry.

INTRODUCTION

Light diffraction studies of muscle fibers are done to gain new information about muscle structure not available through light microscopy. The diffraction pattern produced by a single skeletal muscle fiber is characterized by a zero-order line on a plane perpendicular to the fiber axis and higher-order lines ($m = 1, 2, 3 \ldots$) parallel to but diffracted above and below the zero-order line. Because the single muscle fiber has a relatively large diameter, d, when compared with the wavelength, λ, of the light diffracted ($d \gg 1\ \mu m > \lambda$), the resolution of zero-order structure is usually too low to provide accurate information about the fiber diameter. The higher orders diffracted above and below the zero-order plane are of greater interest, and consequently much work has concentrated on the line widths of the various diffraction orders and their intensities.

Various data acquisition techniques have used film (Cleworth, 1972; Sandow, 1936) and highly sophisticated, rapid digital computing systems (Roos et al., 1980). The intensity distributions of the first order, and to a lesser extent the second and third, give information about the mean sarcomere length during rest and activation. The regular light and dark striations (A and I bands) of skeletal muscle fibers (Ranvier, 1874; Huxley and Hanson, 1954; Huxley, 1957) account for the distinctive diffraction pattern that was originally described by the simple plane grating equation $m\lambda = d \sin \beta$, where m equals order, λ equals wavelength, β equals angle of diffraction, and d equals sarcomere length (the A-I band striation spacings). However, recent studies, having shown the inadequacy of the simple grating equation, proposed more complex theories and models. Investigators such as Fujime (1975), Rüdel et al. (1977), and Baskin et al. (1979) attributed a three-dimensional grating effect to the fiber. Furthermore, Lieber et al. (1981), Lieber and Baskin (1982), Oba et al. (1981), Baskin et al. (1980), Yeh et al. (1980), Rüdel and Zite-Ferenczy (1978, 1979, 1980) consider Bragg reflections in addition to the three-dimensional model.

Our work examines the entire diffraction pattern (orders zero through four) from single glycerinated resting skeletal muscle fibers, photographically and photoelectrically, as a function of rotation about the fiber axis. We show that any one fiber in a particular orientation is a special case and will not yield complete information about fiber morphology. We will treat diffraction as a special case of scattering from ordered structures.

MATERIALS AND METHODS

Extraction and Preparation of Individual Muscle Fibers

Semitendinosus muscle of double pithed southern grass frogs (*Rana pipiens*) was used in the experiments. The following sequence of steps produced intact, single, glycerinated fibers.

Step 1. Preparation of whole muscle. The whole muscle was exposed using stainless steel razor blades and forceps (H5; DuPont Instruments, Wilmington, DE) under a dissecting microscope. Both ends of the whole muscle bundle were tied with suturing thread, subsequently pulled apart to taut and permanently fixed at this length. The dissection was performed in Ringer's solution consisting of (in millimoles per liter): NaCl, 115; KCl, 2.5; $CaCl_2$, 1.8; Na_2HPO_4, 2.15; NaH_2PO_4, 0.85; the pH was adjusted to 7.0. From this whole muscle, several 1–2 mm thick slices of fiber bundles cut lengthwise were separated and kept at the original length.

Step 2. Glycerination of muscle. Fast-glycerinated preparations were employed according to procedures outlined by Rome (1972). Immediately after excision from the frog, the 1–2 mm thick fiber bundles were stored at 0°C. They were then osmotically shocked by alternating them four to five times between a standard salt solution (100 mM KCl, 5

Mr. Gilliar's present address is College of Osteopathic Medicine, Michigan State University, 319 E. Fee Hall, East Lansing, Michigan 48824.

mM $MgCl_2$, 10 mM $AgNPO_3$, 10 mM phosphate buffer, pH 7.0) and the glycerol solution (50% vol/vol glycerine and standard solution). The membranes break down quickly, leaving the gross structure of the contractile apparatus unaffected (Szent-Györgyi, 1949). The preparations were stored in the deep freeze and ready for use 2–4 d after extraction. Identical fresh salt solutions were used throughout the diffraction experiment.

Step 3. Single fiber preparation. The preparation of a single glycerinated fiber involved several steps. A previously prepared 1–2 mm slice was pulled into two equal halves lengthwise. It was decided before hand to permanently fix one of the halves (i.e., upper-half) with fine surgical forceps. The end of the other half was then pulled away as far as possible. The adjoining rest was further disconnected by pushing apart the stationary upper-half carefully with very fine scalpels. This leaves the lower-half of the slice untouched over most of its length as the above procedure is continued until finally one single fiber has been isolated. The fibers selected ranged between 60–85 μm in diameter. The sarcomere length was not changed and measured 2.5 μm.

Preparation and Mounting for Scattering Experiments

The single fiber was transferred onto a microscope slide with a drop of saline solution and was inspected under the light microscope to ensure that it was free from imperfections such as bends, breaks, twists, or adhering particulates. The microscopic appearance of our individual muscle fibers used for the scattering experiments was similar to those shown by Gould (1973). In his photographs, the skew angles are clearly visible. We did not make a concurrent microscopic study to relate skew angle and scattering tilt with rotation. One end of the intact fiber was then glued with fast setting glue onto a hand-drawn glass rod tapered to 50 μm, while the other end was glued to a thin lightweight plastic weight (<5 mg). In all cases, the weight stretched the fiber no more than 1% of its original length. Both glass rod and plastic weight had been fastened to the slide with small alligator clamps. The entire slide with the fiber attached was then immersed into the scattering chamber (18 cm by 12 cm by 14 cm) filled with the standard salt solution. The glass rod on top was permanently fixed to an x-y-z-θ-ϕ translator for micro-manipulation of the fiber. When the alligator clamps and microscope slide were removed, the fiber hung freely in solution, in a vertical, taut but unstretched position. With care, virtually all fibers prepared this way were suitable for light-scattering studies.

EXPERIMENTAL SETUP

The experimental setup is shown in Fig. 1. Unpolarized light from a 0.5 mW HeNe (λ6,328 Å) laser, directed horizontally through an optically perfect glass entrance window of the scattering tank, strikes and is scattered by the muscle fiber hanging vertically in saline solution. The laser light is scattered by the fiber into angles θ and β through the optically perfect glass exit window and is displayed on a screen or recorded on film. A ϕ-wheel connected to the x-y-z translator can rotate the fiber 360° about its z-axis perpendicular to the horizontal plane, while keeping the fiber exactly centered in the laser beam. The fiber can also be translated along its z-axis.

Light scattered by the fiber forms diffraction patterns characteristic of known fiber geometry. The θ-scattering occurring in a plane perpendicular to the z-axis is characteristic of scattering by a cylindrical fiber. The intensity $I(\theta)$ is a function of its diameter and optical constants

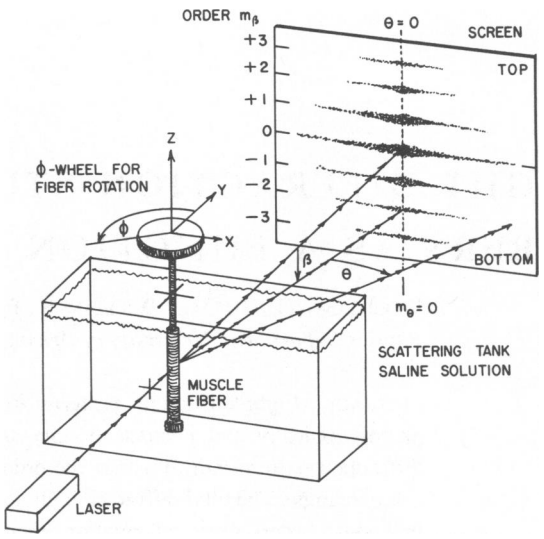

FIGURE 1 Geometrical arrangement of laser beam, muscle fiber, scattering tank, and viewing screen to study light scattering from a muscle fiber. The cylindrical fiber scatters in the θ-direction, the sarcomeres scatter in the β-direction. The ϕ-wheel rotates the fiber about its vertical z-axis.

(refractive index and absorption). The β-scattering occurring above and below the fiber scattering plane at quantized β-locations is characteristic of periodic disturbances along the fiber axis. The intensity $I(\beta)$, which is dominated by diffraction and which reaches a maximum at various orders, yields information about the periodicity, orientation, and spatial frequency of these disturbances (Bickel et al., 1980).

The screen, placed 80 cm from the fiber, consisted of either a white paper for viewing by eye, a photographic paper for direct recording of the entire $I(\theta\beta)$ scattering pattern, or a high quality ground glass screen through which photoelectric measurements could be made. The above experimental set up permitted quantative measurement of virtually all of the light scattered from the fiber into θ and β as a function of fiber translation and rotation.

EXPERIMENTAL MEASUREMENTS

Photographic Studies

Our studies of several muscle fibers showed that the scattered light was indeed strongly dependent on fiber rotation ϕ about the z-axis. This is convincingly demonstrated by the four photographs of the scattering patterns from the same fiber for four different ϕ rotations (separated by 90°) shown in Fig. 2. These photographs demonstrate four aspects of the light-scattering patterns: $\phi = 0$, no tilt, bottom orders brightest; $\phi = 180°$, no tilt, top orders brightest; $\phi = 90°$, maximum tilt counterclockwise; and $\phi = 270°$, maximum tilt clockwise. Similar photographs taken at $\phi = 10°$ intervals to obtain ϕ rotation data show intermediate tilt angles and intensities for various orders.

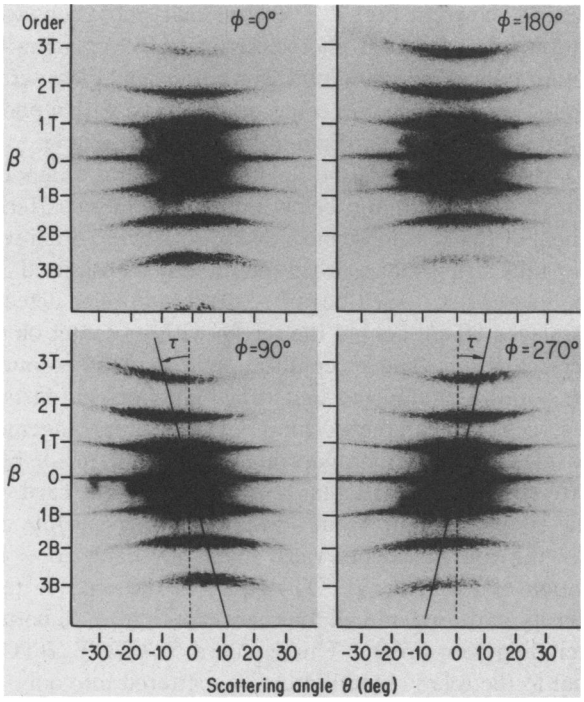

FIGURE 2 Photographs of muscle fiber scattering patterns at four different θ-angles. Sarcomere scattering occurs vertically in the β-direction, cylindrical fiber scattering occurs horizontally in the θ-direction. At $\phi = 0°$ and 180° the scattering is symmetric in $\pm\ \theta$, while the TOP and BOT orders have exchanged maximum brightness. At $\phi = 90°$ and 270° the scattering is symmetric about $\pm\ \beta$, while a tilt occurs in the location of successive order maxima.

The photograph for $\phi = 0$ of Fig. 2 shows the well-known scattering pattern from a striated muscle fiber. Scattering in the $\pm\ \theta$ direction of zeroth β-order is a function of the fiber diameter d, and for small perfect fibers can yield accurate information about fiber diameter and cross-sectional geometry (Bell and Bickel, 1981). Of greater interest and what is emphasized in this study is the quantized β-scattering (diffraction), above and below the zero-order plane, which yields information about the sarcomere spacing. From the grating equation $m\lambda = d \sin \beta$, where m is the β-order number, λ is the wavelength in saline, and β is the scattering (diffraction) angle, we obtain $d = 2.5\ \mu$m for the sarcomere spacing, a value consistent with the one obtained from microphotographs. We call attention to the increasing curvature of increasing β-order patterns, an artifact due to astigmatism at the plane glass exit window of the scattering chamber. The value for β used in the grating equation has been corrected to account for Snell's law of refraction of the diffracted rays leaving the exit window. In the photograph for $\phi = 0$ of Fig. 2, additional sarcomere structure information is contained in the intensity variations of various β-order diffraction. For example, the bottom orders are brighter than the top. Quantitative measurements of these intensity variations are discussed in the next section.

The photograph for $\phi = 180°$ shows a scattering pattern similar to $\phi = 0°$ except here the top orders are brighter than the bottom. More striking is what occurs as the fiber is rotated from $\phi = 0°$ to 360°. The scattering pattern displays a tilt τ that reaches a maximum of 14° at $\phi = 90°$ and $\phi = 270°$ as shown in Fig. 2. At these angles, the intensity distribution is essentially symmetric in the β-direction; equivalent top and bottom orders are approximately equal in intensity. The tilt angle for any ϕ is determined directly with a protractor that measures the angle between the solid line, passing through the maximum intensity point of each order, and the dotted vertical line. Because the fiber lacked any internal anatomical hallmark that could be used as a reference for the rotation angle ϕ, the starting point of the rotation ($\phi = 0$) was arbitrarily chosen. We assigned $\phi = 0$ to the fiber orientation that produced a zero tilt angle when the bottom orders were brighter than the top orders.

The tilt is caused by slanted parallel sarcomere planes as demonstrated in Fig. 3. The parallel planes T, tilted an angle τ to the horizontal scattering plane H, act as scattering centers that diffract the light in a direction perpendicular to the planes. The vertically aligned fiber scatters light in the θ-direction perpendicular to the fiber. The combined result is cylindrical fiber scattering in the θ-direction and sarcomere scattering (diffraction) in the β-direction, but tilted through an angle τ that depends on fiber rotation ϕ. A spiral geometry does not produce a ϕ-dependent tilt. Although a spiral scatters light above and below the $\beta = 0$ plane, its geometry is independent of ϕ. It creates symmetric herringbone or cat's whisker scattering patterns, which are also independent of ϕ (Bickel et al., 1980).

Fig. 4 shows the geometrical relationship between ϕ and τ. Here z is the fiber axis, τ is the tilt angle, L is the face

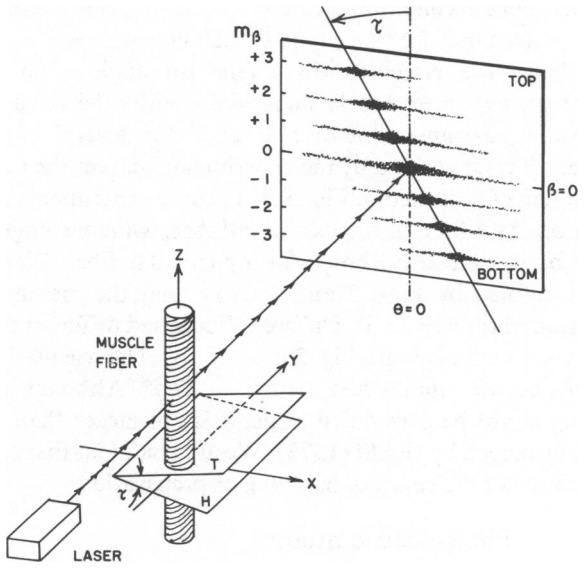

FIGURE 3 Geometrical arrangement of laser beam, fiber, sarcomere planes, and viewing screen to show the origin of the scattering pattern tilt. The sarcomere tilt τ oriented at $\phi = 90°$ gives rise to the $\phi = 90°$ tilt pattern shown in Fig. 2.

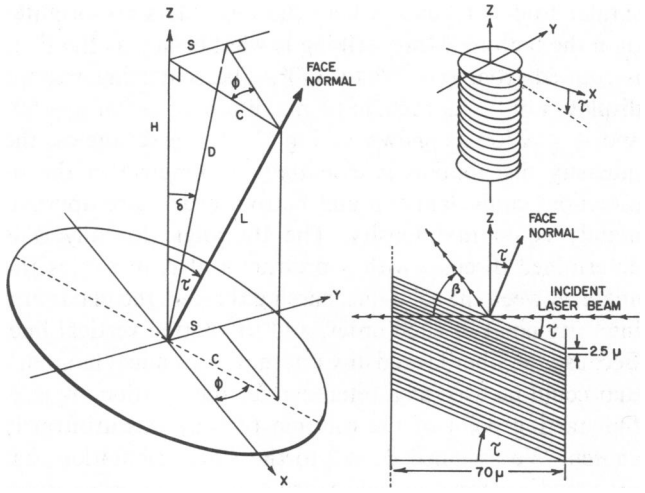

FIGURE 4 (*Left*) The relationship among the sarcomere tilt angle τ, fiber rotation angle ϕ, and the projection of τ on to the plane perpendicular to the laser beam. (*Right* top) The geometrical arrangement of sarcomere planes tilted through τ. (*Right* bottom) The relationship between the sarcomere tilt angle τ, β-scattering, and the blaze angle. When $\beta = 2\tau$, the incident radiation is both reflected from and scattered by the sarcomere faces giving enhanced intensity in the blaze direction β. The figure is drawn approximately to scale showing the relative sizes of sarcomere spacings (2.5 μm), fiber diameter (70 μm) and tilt angle (22.5°).

normal, H is the projection of L on the fiber axis, ϕ is the fiber rotation angle, and δ is the projection of τ in the plane perpendicular to the laser-beam axis y. When δ reaches a maximum, the tilt of the diffraction pattern equals the tilt of the sarcomere planes. Note that H, L, and τ are constant. From the geometry we have $D \sin \delta = C \sin \phi$ and $D \cos \delta = H$, which yields $\tan \delta = C/H \sin \phi = \tan \tau \sin \phi$, so that $\delta = \text{arc tan } [\tan \tau \sin \phi]$. For one particular set of experimental conditions, where $\tau = 22.5°$, this becomes $\delta = -\text{ arc tan } [22.5° \sin \phi] = -22.5° \sin \phi$ or $\tau = -\tau_m \sin \phi$. Thus, the projected tilt δ (the tilt angle τ on the photograph) varies nearly sinusoidally with ϕ between the constant sarcomere tilt of $\tau = 22.5°$ for several of our fibers. This is verified by the experimental curves for τ as a function of ϕ plotted in Fig. 5 *A*. In these experiments τ_{max} is a constant for a particular initial fiber, while the angle ϕ has been arbitrarily chosen for a particular fiber orientation defined by Figs. 2 and 4. Note that the maximum measured tilt was 22.5°. Different fibers had different tilts. The one used to obtain Fig. 2 has $\tau = 14°$. The one used for photoelectric studies had a tilt $\tau = 22.5°$. Although this value might be considered large, it is not larger than the one displayed by Gould (1973). We are confident that such tilts are not the result of handling or preparation.

Photoelectric Studies

In addition to the ϕ-dependent tilt of the diffraction patterns, a periodic intensity variation occurs in the top and bottom halves of the diffraction pattern (above and below $\beta = 0$), as well as within various individual orders themselves as shown in Fig. 2. These intensity variations were quantatively measured photoelectrically by replacing the photographic paper with a translucent ground glass screen through which intensities could be measured with a photomultiplier detector. The data are presented in Fig. 5.

Our main interest is the light scattered into orders one through four above and below the $\beta = 0$ fiber scattering plane. For this reason we blocked the entire zero order with an opaque strip that absorbed the directly transmitted and near forward scattered beam. A photomultiplier detector was placed 80 cm behind the screen with its center on the laser-beam axis. The acceptance angle of the photomultiplier optics was adjusted to accept light from all parts of the screen with equal efficiency. This optical arrangement measured intensities proportional to the amount of light scattered into any particular β order. An opaque card was used to block light from unwanted orders, while the following measurements were made for each $\phi = 10°$ rotation of the fiber. I(TOT) equal to the relative total intensity scattered into all four orders both top and bottom (excluding zero order). This is curve 5 *B* TOT. I(TOP) equal to the relative total intensity scattered into only the top four orders. This is curve Fig. 5 *C* TOP. I(BOT) equal to the relative total intensity scattered into only the bottom four orders. This is curve Fig. 5 *C* BOT.

We make the following observations. First, the total intensity (TOT) scattered by the fiber into θ and β (excluding zeroth order) shown in Fig. 5 *B* oscillates according to $I \doteq -I_o \sin 2\phi$ demonstrating that the fiber does not have a circular symmetric cross section. Second, the intensities scattered into the upper-half (TOP) and lower-half (BOT) of the diffraction patterns shown in Fig. 5 *C* are out of phase by ~180°. The sums of the TOP and BOT intensities, I(TOP) + I(BOT), indicated as small circles in Fig. 5 *B*, almost coincide with the total measured intensity I(TOT) $\equiv$ I(TOP + BOT) = I(TOP) + I(BOT) indicating that all of the light was accounted for in these measurements.

Third, the intensity of the brightest portion of each particular order was measured as a function of θ. To do this a small equal portion of each order near the maximum was scanned with the photomultiplier, and the maximum intensity was recorded. These data are displayed in Fig. 5 *D*, which shows the variation of the first-order TOP and BOT; Fig. 5 *E*, which shows the variation of the second-order TOP and BOT; and in Fig. 5 *F*, which shows the variation of the third-order TOP and BOT and fourth-order TOP and BOT. Note these intensities are not the same as the total intensity measurements of Fig. 5 *B* and *C*.

In all cases, the intensity varies periodically with ϕ but with a phase difference of ~180° between the top and bottom curves. All measurements are averages over at least four full ϕ-rotations of the fiber, and fluctuations are <5% at any angle. The solid lines, which connect the experimental points, are intended only to guide the eye. The deviations from perfectly symmetric smooth curves that might

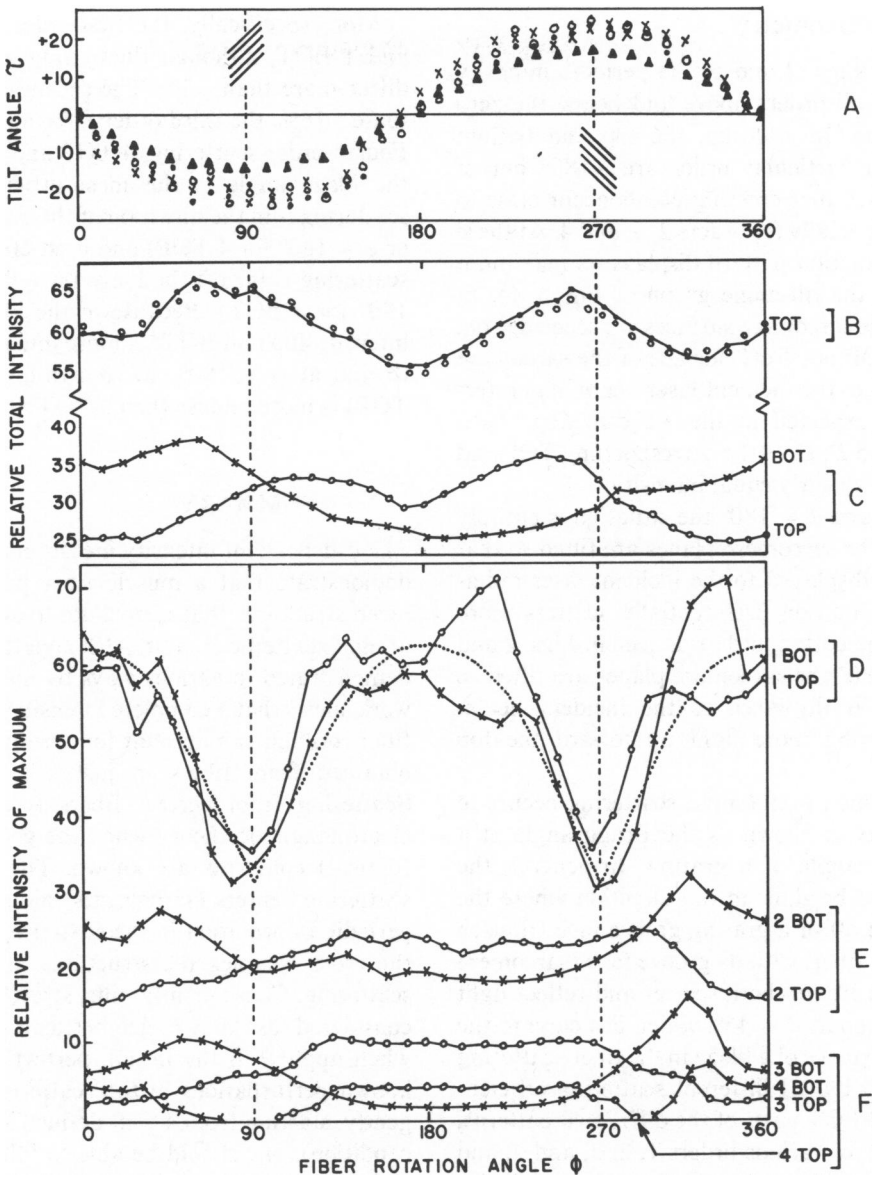

FIGURE 5 Projected tilt and intensity variations of the light scattered into various orders of the fiber diffraction pattern as a function of fiber rotation angle ϕ. Note that all ϕ data are taken at 10° intervals. (*A*) Diffraction pattern tilt as a function of ϕ for several fibers. The parallel lines at $\phi = 90°$ and 270° represent the orientation of sarcomere planes as seen by the incident laser beam. (*B*) Total intensity scattered into all orders (excluding zero order). The dotted line connects the points of total measured intensity, the small circles are the sums of the independently measured TOP and BOT orders of *C* below. (*C*) The total intensity scattered into all four orders above $\beta = 0$ (TOP) and below $\beta = 0$ (BOT). (*D*) The variation of the intensity maximum for the first-order TOP and BOT. The dotted line represents the mathematical function $I = I_0|\cos\phi|$. (*E*) The variation of the intensity maximum for the second-order TOP and BOT. (*F*) The variation of the intensity maximum for the third- and fourth-order TOP and BOT.

be expected are due to an imperfect muscle fiber, not noise in the intensity measurements.

INTERPRETATION AND RESULTS

Fiber Symmetry

The photographic and photoelectric data presented in Figs. 2 and 5 demonstrate that our single muscle fibers are not cylindrically circular symmetric. Consequently, an $I(\theta\beta)$ study of such a fiber mounted at some random ϕ giving a scattering pattern for only one orientation ϕ could be devoid of certain geometrical information. A single fiber mounted on a microscope slide could be flipped 180° but would give information for only two orientations of ϕ corresponding to a set of data points that lie along two vertical lines located at ϕ and $\phi + 180°$ of Fig. 5. In addition, this kind of geometry destroys the cylindrical symmetry of a perfect fiber if the fiber is in contact with a flat glass surface.

Sarcomere Geometry

As demonstrated in Figs. 2 and 5, the periodic intensity variations occur for all orders above and below the zero order ($\beta = 0$) plane. In addition, the top and bottom components of each particular order are ~180° out of phase. First, we notice that crossing points occur close to $\phi = 90°$ and 270°, especially for orders 2, 3, and 4. At these angles the fiber diffraction pattern displays its maximum tilt (as indicated in the tilt-angle graph of Fig. 5 *A*). In these orientations, the sarcomere surfaces are seen edge on. Since neither the TOP nor BOT surface of the sarcomere planes displays itself to the incident laser beam, no preferential scattering is expected in the $\pm\beta$ direction. As a result, in Figs. 2 and 5 *D*, *E*, *F*, the corresponding TOP and BOT orders have very nearly equal intensity.

At angles $\phi = 0°$ and $\phi = 180°$ the situation is entirely different. At $\phi = 0$ the sarcomere planes are tilted so that their bottom side is displayed to the incident laser radiation. This plane orientation preferentially scatters more light down toward the bottom orders as seen in Figs. 2 and 5 *D*, *E*, *F*. At $\phi = 180°$ the sarcomere planes are tilted so that their top side is displayed to the incident beam, preferentially scattering more light up toward the top orders.

This angle into which preferential scattering occurs to enhance the intensity is known as the Bragg angle of a crystal or the blaze angle of a grating. In general, the diffracted intensity is brighter in the direction where the radiation is reflected off of a grating groove face (Bausch and Lomb, 1977). A fiber, with its groove face (sarcomere plane), tilted $\tau = 22.5°$, will both scatter and reflect light into the blaze direction at $\beta = 45°$, which lies close to the fourth order. The existence of a blaze in the fiber scattering data is demonstrated by (*a*) different scattering efficiencies for the TOP and BOT parts of the diffracted patterns, (*b*) intensity changes of various orders 1, 2, 3, and 4, and (*c*) different percentage intensity changes of a particular order as a function of fiber rotation.

The fourth order of 6,328 Å lying at 45°, close to the blaze wavelength, is more influenced by it than the orders one, two, and three that lie at angles <45° and off the blaze. The first-order intensity being off the blaze is governed by the efficiencies of scattering from the fiber. In the best of cases involving high quality gratings, the theoretical intensities agree with experiment only approximately because of irregularities in the groove surfaces and polarizations. It is not a rule that first order must be more or less intense than a higher order that lies on the blaze. Consequently the intensity distribution of the various orders is not as good as indicator of the blaze as is the change in I that occurs by going off the blaze. The fourth order, being in the blaze suffers the largest fractional intensity change when the fiber is rotated to put fourth order out of the blaze. First order suffers only little.

More specifically, the first-order intensities at 1 TOP and 1 BOT, although fluctuating greatly with ϕ do not differ more than ~3%. The second-order intensities fluctuate ~16%, the third order 80%, and fourth order >80%. Fourth-order scattering, 4 TOP and 4 BOT, lying close to the blaze angle is the most efficient of all when the scattering is in the direction of the blaze ($\phi = 0°$ for 4 BOT or $\phi = 180°$ for 4 TOP) and least efficient of all when the scattering is far off the blaze ($\phi = 0°$ for 4 TOP and $\phi = 180°$ for 4 BOT). Because of the blaze, the fourth-order intensity BOT (4 BOT) is more intense than 3 TOP at $\phi = 0°$ and at $\phi = 180°$, the fourth-order intensity TOP (4 TOP) is more intense than 3 BOT at $\phi = 180°$.

SUMMARY

The ϕ-dependent intensity measurements and their results demonstrate that a muscle fiber possesses certain organized structures that contribute to an orderly distribution of light scattered from it. Although these effects have been demonstrated in various ways by many investigators, this work shows that a complete intensity study as a function of fiber rotation can account for certain randomness in data obtained from fibers in just one or two orientations. Scattering from perfect fibers is exactly predicted by electromagnetic theory when the geometry and electrical (optical) constants are known. The addition of periodic scattering centers (sarcomeres) along the fiber axis adds periodic information in the scattering pattern. In general, the more complex the structures, the more complex the scattering. Consequently, tilts, stretches, and twists can be considered as known geometrical perturbations, which when applied to the initial, perfect structure will create known perturbations in the scattering. While perturbing gently, starting from a well-defined starting point (resting condition), one should be able to follow the $I(\phi\beta)$ signals and learn unique information about the fiber. Unfortunately, no fiber is perfect in geometry or in homogeneity of its optical constants. Such geometrical distortions will thus distort the expected perfect $I(\phi\beta)$ pattern and, in general, scatter light more randomly than desired. Small Rayleigh scatterers attached to or immersed in larger Mie systems or in very regular structures add a Rayleigh component to the scattering causing an overall loss in contrast of the scattering signal (Bickel et al., 1982). Large Mie structures randomly dispersed and orientated throughout the scatterer create random intensity maxima and minima (noise) that can obscure or confuse the information scattered from the periodic structure of interest. Because scattering data in general are complex and extremely sensitive to geometrical and optical features, it is important to manipulate these features as much as possible, but only to the extent that their signals are meaningful and interpretable. With these contributions accounted for, what is

left can be attributed to the properties of the scatterer itself.

We appreciate the assistance and many helpful conversations with Drs. David J. Hartshorne of Nutritional and Food Sciences, Peter E. Pickens of Cell and Developmental Biology, and Howard D. White of Biochemistry, all of the University of Arizona. We also acknowledge support of the University of Arizona Biomedical Research Grant Committee.

Received for publication April 5 1983.

REFERENCES

Baskin, R. J., R. L. Lieber, T. Oba, and Y. Yeh. 1980. Intensity of light diffraction from striated muscle as a function of incident angle. *Fed. Proc.* 39:1729 (Abstr.)

Baskin, R. J., K. P. Roos, and Y. Yeh. 1979. Light diffraction study of singles skeletal muscle fibers. *Biophys. J.* 28:45–64.

Bausch and Lomb. 1977. Diffraction Grating Handbook 1–49.

Bell, B. W., and W. S. Bickel. 1981. Single light scattering matrix: an experimental determination. *Appl. Opt.* 20:3874–3879.

Bickel, W. S., W. G. Gilliar, and B. Bell. 1980. Light scattering from fibers: A closer look with new twist. *Appl. Opt.* 19:3671–3675.

Bickel, W. S., H. A. Yousif, and W. M. Bailey. 1982. Masking of information in light scattering signals from complete scatterers. *Aersol Sci. Technology.* 1:329–335.

Cleworth, D. R., and K. A. P. Edman. 1972. Changes in sarcomere length during isometric tension developments in frog skeletal muscle. *J. Physiol. (Lond.).* 227:1–17.

Fujime, S. 1975. Optical diffraction study of muscle fibers. *Biochim. Biophys. Acta.* 379:227–238.

Gould, R. P. 1973. The microanatomy of muscle. *In* The Structure and Function of Muscle. G. H. Bourne, editor. Academic Press, Inc., New York. Second ed. 2:185–241.

Huxley, H. E. 1957. The double array of filaments in cross-striated muscle. *J. Biophys. Biochem. Cytol.* 3:631–648.

Huxley, H. E., and J. Hanson. 1954. Changes in the cross-striations of muscle during contraction and stretch and their natural intepretation. *Nature (Lond.).* 173:973–976.

Lieber, R. L., Y. Yeh, and R. J. Baskin. 1981. The use of laser diffraction to measure sarcomere length. *Biophys. J.* 33:(2, pt.2) 223*a*. (Abstr.)

Lieber, R. L., and R. J. Baskin. 1982. Intensity of first order diffracted lines after quick stretch/release of single muscle fibers. *Biophys. J.* 37 (2, pt. 2):365*a*. (Abstr.)

Oba, T., R. J. Baskin, and R. L. Lieber. 1981. Light diffraction studies of active muscle fibers as a function of sarcomere length. *J. Muscle Res. Cell Motil.* 2:215–224.

Ranvier, L. 1874. Du spectre par les muscles striés. *Arch. de Physiol. T.* 6:774–775.

Rome, E. 1972. Structural studies by x-ray diffraction of striated muscle permeated with certain ions and proteins. *Cold Spring Harbor Symp. Quant. Biol.* 37:331–339.

Roos, K. P., R. J. Baskin, R. L. Lieber, J. W. Cline, and P. J. Paolini. 1980. Digital data acquisition and analysis of striated muscle diffraction patterns with a direct memory access microprocessor system. *Rev. Sci. Instrum.* 51:762–767.

Rüdel, R., and F. Zite-Ferenczy. 1977. Intensity behavior of light diffracted by single frog muscle fibers from narrow laser beams. *J. Physiol. (Lond.).* 272:31P–32P.

Rüdel, R., and F. Zite-Ferenczy. 1978. Bragg-reflexion by cross-striated frog muscle. *J. Physiol. (Lond.).* 284:99P–100P.

Rüdel, R., and F. Zite-Ferenczy. 1979. Interpretation of light diffracted by cross-striated muscle as Bragg reflexion of light by the lattice of contractile proteins. *J. Physiol. (Lond.).* 290:317–330.

Rüdel, R., and F. Zite-Ferenczy. 1980. Efficiency of light diffraction by cross-striated muscle fibers under stretch and during isometric contraction. *Biophys. J.* 30:507–516.

Sandow, A. 1936. Diffraction pattern of frog sartorius and sarcomere behavior during contraction. *J. Cell. Comp. Physiol.* 9:37–54.

Szent-Györgyi, A. 1949. Free-energy relations and contraction of actomyosin. *Biol. Bull.* 96:140–161.

Yeh, Y., R. J. Baskin, R. L. Lieber, and K. P. Roos. 1980. Theory of light diffraction by single skeletal muscle fibers. *Biophys. J.* 29:509–522.